THE JOURNAL OF PHYSICAL CHEMISTRY B

Article

Cite This: J. Phys. Chem. B 2019, 123, 5181−5188

pubs.acs.org/JPCB

Dynamic Heterogeneities in Colloidal Supercooled Liquids: Experimental Tests of Inhomogeneous Mode Coupling Theory

Published as part of The Journal of Physical Chemistry virtual special issue "Hai-Lung Dai Festschrift".

Chandan K. Mishra,[†] Piotr Habdas,[‡] and A. G. Yodh*[,†]

[†]Department of Physics and Astronomy, University of Pennsylvania, Philadelphia, Pennsylvania 19104, United States

[‡]Department of Physics, Saint Joseph's University, Philadelphia, Pennsylvania 19131, United States

Supporting Information

ABSTRACT: The dynamics in supercooled liquids slow enormously upon approaching the glass transition, albeit without significant change of liquid structure. This empirical observation has stimulated development of many theoretical models which attempt to elucidate microscopic mechanisms in glasses and glass precursors. Here, quasi-two-dimensional colloidal supercooled liquids and glasses are employed to experimentally test predictions of widely used models: mode coupling theory (MCT) and its important extension, *inhomogeneous* MCT (IMCT). We measure two-point dynamic correlation functions in the glass forming liquids to determine structural relaxation times, τ_α, and mode coupling exponents, a, b, and γ; these parameters are then used to extract the mode coupling dynamic crossover packing area-fraction, ϕ_c. This information, along with our measurements of supercooled liquid spatiotemporal dynamics, permits characterization of dynamic heterogeneities in the samples and facilitates direct experimental tests of the scaling predictions of IMCT. The time scales at which dynamic heterogeneities are largest, and their spatial sizes, exhibit power law growth on approaching ϕ_c. Within experimental error, the exponents of the measured power laws are close to the predictions of IMCT.

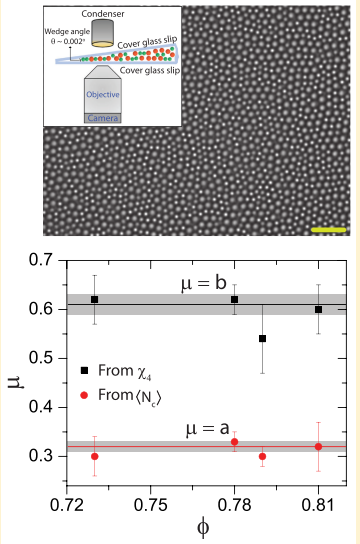

INTRODUCTION

Elucidation of the microscopic origin of dynamic arrest in supercooled liquids and glass precursors remains a key challenge in condensed matter physics and chemistry.[1−11] Slow cooling of a liquid produces crystallization, but rapid cooling can bypass crystallization. In the latter case, the liquid enters into a supercooled regime, and, after further cooling toward the glass transition temperature, T_g, the liquid evolves to a glassy state with solid-like rigidity. Notably, the viscosity, η, or equivalently the structural relaxation time, τ_α, varies by many orders of magnitude in the vicinity of the transition, although little change in static structure is observed.[4,12] In total, findings from experiments and simulations suggest that relaxation processes in supercooled liquids and glasses are cooperative, involving large numbers of constituent particles.[8]

These and other intriguing observations have led to the development of many theoretical models. Among these are the free volume theory,[13,14] energy landscape models,[15,16] configurational entropy theory,[17,18] mode coupling theory (MCT),[19,20] kinetically constrained models,[21] random first-order transition (RFOT) theory,[22−24] and dynamic facilitation theory.[25,26] Each of these models captures aspects of the glass transition. However, a universally accepted complete theoretical description of the glass transition and glasses is still lacking.

Mode coupling theory (MCT) is one of the oldest mean field theories; MCT is a hydrodynamic and coarse grained description of the two-point dynamic correlation function that explains the slowing of structural relaxation in supercooled liquids and glasses.[1,2,19,20,27−29] With the sample static structure factor as its only input, MCT predicts the time-dependent decay profile of the two-point dynamic self-intermediate scattering correlation function, $F_s(\vec{q},t)$. $F_s(\vec{q},t)$ decays exponentially for liquids at high temperature, and it usually exhibits a two-step decay profile for supercooled liquids and glasses. The first decay step is associated with trapping of particles within their nearest-neighbor cages and is called β-relaxation; the second decay step is associated with cage-rearrangements and cage escape and is called α-relaxation.

MCT predicts that $F_s(q, t)$ should decay as a power law with exponents a and b during the early β- and the early α-relaxation regimes, respectively.[2,28−31] Interestingly, a and b are not

Received: April 11, 2019
Revised: May 27, 2019
Published: May 27, 2019

DOI: 10.1021/acs.jpcb.9b03419
J. Phys. Chem. B 2019, 123, 5181−5188

independent, and MCT explicitly predicts their relationship. Moreover, MCT uses these exponents (a and b) and the structural relaxation time scale, τ_α (associated with α-relaxation), to predict an ergodic to nonergodic transition temperature, T_c.[2,28−31] Note, even though T_c is higher than the ideal glass transition temperature T_g,[32] MCT successfully identifies a dynamic crossover temperature which separates the collision dominated regime from the regime dominated by activated dynamics.[4,33−36] MCT captures dynamics in the collision dominated regime within the intermediate range of supercooling. Most experimental studies, especially those employing colloidal suspensions, probe dynamics for temperatures slightly less than T_c (or equivalently for colloids, for packing fractions slightly more than mode coupling crossover packing area-fraction, ϕ_c).

MCT is among the most accessible of theories, and its predictions have been directly tested by many experiments[37−45] and simulations.[46−49] Despite many successes, however, basic MCT cannot explain the pathways for structural relaxation found in supercooled liquids and glasses. These cooperative relaxation events are called dynamic heterogeneities and are typically characterized by the sample four-point susceptibility, $\chi_4(t)$.[1,50−55] To address this limitation, Biroli et al. extended MCT to spatially inhomogeneous systems, for example, to systems with small, localized perturbations. The more sophisticated formalism is called *inhomogeneous* mode coupling theory (IMCT).[56]

In IMCT, the response of the dynamic structure factor to localized small perturbations is computed and expressed as a three-point susceptibility, $\chi_3(t)$, which is closely connected to $\chi_4(t)$ and which exhibits similar time-dependent behavior.[56] Briefly, the magnitude of $\chi_4(t)$ provides a measure of the average size of the cooperatively rearranging regions. $\chi_4(t)$ varies with lag time, t, and its maxima occurs in the α-relaxation regime at $t = \tau_4$; the dynamics are most heterogeneous at this time. Theory predicts that $\chi_4(t)$ should grow as a power law in the early α-relaxation regime, i.e., $\chi_4(t) \propto t^\mu$, and that its peak amplitude, $\chi_4(\tau_4)$, should also follow a power law with τ_4, $\chi_4(\tau_4) \propto \tau_4^\lambda$.[57] Importantly, these power law exponents, μ and λ, can be used to test competing theories of the glass transition. To date, numerical studies of binary systems have investigated the predictions of $\chi_4(t)$ and were found to be in agreement with IMCT.[46,57] However, to our knowledge, these predictions have *never been explored in experiments*.

While most work on these questions has focused on scaling behaviors of the four-point susceptibility ($\chi_4(t)$), dynamic heterogeneities (cooperative rearrangements) in supercooled liquids and glasses can be quantified by other methods and physical quantities. Notable among these is the mean cluster size of fast-particles, $\langle N_c(t)\rangle$.[8,38,58] Like $\chi_4(t)$, $\langle N_c(t)\rangle$ also has its largest magnitude in the α-relaxation regime, i.e., at a time $t = \tau_c$. Although the magnitude of τ_4 and τ_c may vary slightly, and the precise meaning of $\chi_4(t)$ and $\langle N_c(t)\rangle$ may also be slightly different, if dynamic heterogeneities (cooperative rearrangements) are truly a hallmark feature of supercooled liquids and glasses, then one might anticipate that the power law scaling of these two parameters should be similar, and this connection should be explored.

Thus, the goals of the present investigation of quasi-two-dimensional colloidal supercooled liquids are multifold. First, we experimentally quantify the dynamics of the sample via the self-intermediate scattering functions, $F_s(\vec{q},t)$, and we extract the MCT exponents a, b, and γ, as well as the structural relaxation time, τ_α; this information enables estimation of the mode coupling dynamic crossover packing area-fraction, ϕ_c. Second, we quantify dynamic heterogeneities using both the four-point dynamic susceptibility, $\chi_4(t)$, and the mean cluster size of fast moving particles, $\langle N_c(t)\rangle$. Finally, the power law scaling of both $\chi_4(t)$ and $\langle N_c(t)\rangle$ are measured, and the exponents are extracted and compared to theory. Notably, the experimental results are found to be largely consistent with the predictions of IMCT.

EXPERIMENTAL SECTION

The samples are binary colloidal mixtures of polystyrene spheres in water with diameters $\sigma_s = 1.0$ μm and $\sigma_l = 1.3$ μm (Figure 1a). The polydispersity for large and small particles are

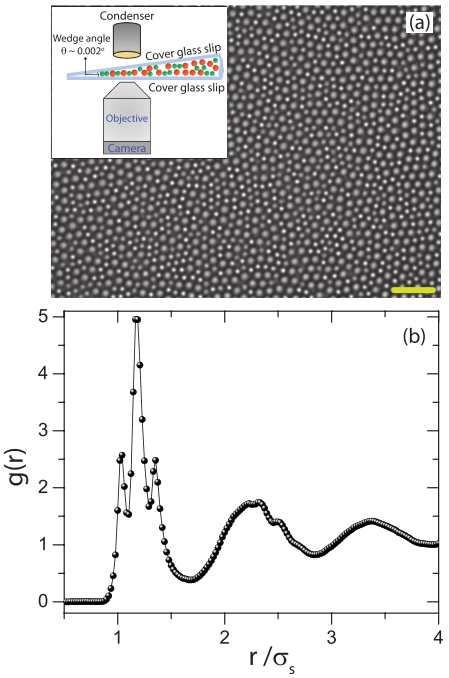

Figure 1. (a) Typical field-of-view shown for a colloidal supercooled liquid sample with $\phi = 0.79$. The scale bar is 10 μm. The inset shows a schematic of the experimental setup; our field-of-view is in the portion of the cell with a layer that is one-particle thick. (b) Static pair correlation function for the sample, $g(r)$, versus particle separation, r, scaled by small particle diameter, σ_s.

5% and 3%, respectively. Use of the binary mixture prevents crystallization, which can be confirmed from the absence of long-range order in the sample pair correlation function $g(r)$ (Figure 1b). The ratio of peak intensities at distances corresponding to small−small and large−large particle separation in $g(r)$, i.e. the first and third peak of $g(r)$, respectively, also shows that the number ratio of small/large particles is approximately unity.

The binary-sphere colloidal suspensions were loaded into a wedged-shaped cell which was left standing to permit particles to sediment into a quasi-two-dimensional (2D) region of the cell (inset to Figure 1a). When a desired area fraction, ϕ, was obtained, the cell was left horizontal on the microscope stage with a typical wait-time of 3−5 h for sample aging/equilibration. Data acquisition followed the sample aging/equilibration. For each ϕ, the particle trajectories were

DOI: 10.1021/acs.jpcb.9b03419
J. Phys. Chem. B 2019, 123, 5181−5188

measured by video microscopy using a 100× oil immersion objective (NA = 1.4) at a frame rate of 4 fps. Depending on ϕ, the experiment duration varied from 25 to 50 min. The center-of-mass trajectories of all particles were tracked, and the data were analyzed using standard MATLAB and Python codes.[59] The area fraction was estimated using $\phi = \left[N_s\pi\left(\frac{\sigma_s}{2}\right)^2 + N_l\pi\left(\frac{\sigma_l}{2}\right)^2\right]/A$, where N_s and N_l is the number of small and large particles, respectively, and A is the total area in the field-of-view. The range of ϕ is $0.56 \leq \phi \leq 0.81$, and $\frac{N_s}{N_l} = 1.00 \pm 0.10$.

RESULTS AND DISCUSSION

Determination of MCT Scaling Exponents: *a*, *b*, and *γ*. First, we experimentally quantify sample dynamics as a function of area fraction, ϕ, using the self-intermediate scattering function $F_s(\vec{q}, t)$. $F_s(\vec{q}, t) = \frac{1}{N}\langle\sum_k^N \exp(\vec{q}\cdot\vec{r}_k(t + t_0) - \vec{r}_k(t_0))\rangle$. Here, $\vec{r}_k$ is the position of the k^{th} particle, $\langle\ \rangle$ denotes average over all particles for all initial times t_0 and a particular lag time t. $\vec{q}$ is the spatial wavevector. Typically, $\vec{q}$ is chosen such that $q = 2\pi/\sigma$, where σ corresponds to a peak position in the radial pair-correlation function, $g(r)$.

Figure 2(a) shows $F_s(q,t)$ at different ϕ for $q = 2\pi/\sigma_s$, where σ_s corresponds to position of the first peak in $g(r)$. The dynamics are diffusive at low area fractions, $\phi < 0.66$; these diffusive dynamics are reflected by the exponential decay of $F_s(q,t)$. For $\phi > 0.66$, the caging of particles at intermediate lag times becomes evident as a plateau in the self-intermediate scattering function. At still longer lag times, the cages rearrange, the particles diffuse out of their respective cages, and $F_s(q,t)$ decays to zero. By convention, the time at which $F_s(q,t)$ decays to $1/e$ is defined as the structural relaxation time, τ_α (indicated by the dotted horizontal line in Figure 2a).

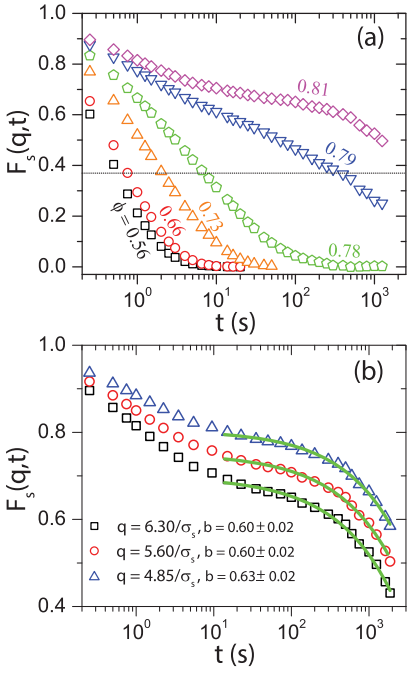

Figure 2. (a) Temporal evolution of self-intermediate scattering function, $F_s(q,t)$, for different packing area fractions, ϕ. q corresponds to the first peak position in pair-correlation function, $g(r)$. The dotted horizontal line is drawn at $F_s(q,t) = 1/e$; its intersection with $F_s(q,t)$ at each ϕ yields the (long-time scale) structural relaxation time, τ_α, for each ϕ. (b) $F_s(q,t)$ versus lag time, t, for three different values of q, corresponding to first three peaks of $g(r)$, at $\phi = 0.81$. The inset shows fitting of von Schweidler law, $F_s(q,t) = f_q - h_q t^b$, (green lines) that determines the von Schweidler exponent $b = 0.61 \pm 0.02$.

Mode coupling theory (MCT) predicts that τ_α diverges upon approach of the mode coupling crossover packing area fraction, ϕ_c. Specifically, MCT predicts $\tau_\alpha \propto (\phi_c - \phi)^{-\gamma}$. Here γ is a system-dependent scaling exponent that depends on two mode coupling exponents a and b, i.e., $\gamma = \frac{1}{2a} + \frac{1}{2b}$. The MCT power law exponents, a and b, help to capture the variation of the self-intermediate scattering function in different time regimes. Fitting to the so-called critical decay law, $F_s(q,t) = f_q + h_q t^{-a}$, in the vicinity of the early β-relaxation time scale provides information about a. Fitting to the von Schweidler law, $F_s(q,t) = f_q - h_q t^b$, in the vicinity of the early α-relaxation time scale provides information about b. Note, f_q and h_q are constants that depend on the plateau height and the amplitude of $F_s(q,t)$, respectively.

Ideally, a and b can be determined by fitting power laws to these early and later time regimes, respectively. For our data, the plateau is most obvious at $\phi = 0.81$ (Figure 2a). Therefore, we use this $\phi = 0.81$ to estimate the exponent b by fitting power laws to decay of $F_s(q,t)$ (Figure 2(b)). We employ three different values of q, corresponding to the first three peaks of $g(r)$, and we fit the decay of the three corresponding $F_s(q,t)$ to determine b. From these, we find $b = 0.61 \pm 0.02$ (Figure 2b).

We were unable to resolve the early time decay of $F_s(q,t)$ prior to the plateau well enough to permit direct fitting for a. However, a can still be determined using yet another remarkable prediction of MCT that connects the exponents a and b using the gamma function: $\frac{\Gamma(1-a)^2}{\Gamma(1-2a)} = \frac{\Gamma(1+b)^2}{\Gamma(1+2b)}$. This relation gives the exponent $a = 0.32 \pm 0.01$, and these values of a and b yield the exponent $\gamma = 2.43 \pm 0.02$.

Determination of the MCT Crossover Packing Area Fraction: ϕ_c. Now that γ is determined, we can use measurements of τ_α to derive the MCT crossover packing area-fraction, ϕ_c. Figure 3 shows plots of $\tau_\alpha^{-1/\gamma}$ versus ϕ for three different values of q (corresponding to the first three peaks of $g(r)$). For all three q values, and for $\phi \geq 0.65$, we see that $\tau_\alpha^{-1/\gamma}$ varies linearly with ϕ. According to MCT, the intersection of these lines with the horizontal axis yields the

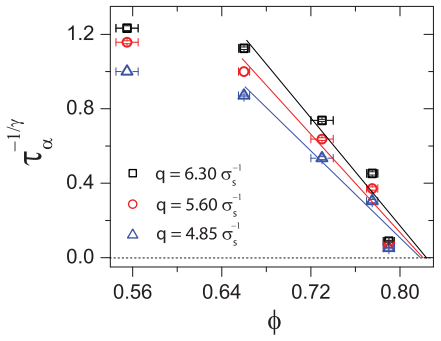

Figure 3. $\tau_\alpha^{-1/\gamma}$ versus ϕ for the three different values of q, corresponding to the first three peaks of $g(r)$. The solid lines are linear fits to the data. The intersection of the fitted lines with the horizontal axis (indicated by horizontal dotted lines) yields the mode coupling crossover area-fraction, $\phi_c = 0.82 \pm 0.01$.

DOI: 10.1021/acs.jpcb.9b03419
J. Phys. Chem. B 2019, 123, 5181−5188

mode coupling crossover packing area-fraction, $\phi_c = 0.82 \pm 0.01$. MCT is most accurate for intermediate supercooling;[46,60] thus, the observed deviation from linearity of $\tau_\alpha^{-1/\gamma}$ versus ϕ in both the liquid phase ($\phi < 0.65$) and in the deeply supercooled phase ($\phi > 0.78$) is expected. Note also, ϕ_c is in close agreement with a previous colloid experiment in quasi-two-dimensions.[38]

Quantification of Dynamic Heterogeneities. It is not possible to distinguish a liquid from a supercooled liquid based on structure ($g(r)$) alone. However, the *dynamic* self-intermediate scattering function, $F_s(q,t)$, can distinguish liquids from supercooled liquids and glasses, and MCT predicts this transition behavior (via the variation of $F_s(q,t)$) with only $g(r)$ as an input. Despite this success, traditional MCT is unable to make statements about many known properties of supercooled liquids and glasses. Chief among them is dynamic heterogeneity. Dynamic heterogeneities are spatial clusters of particles with high and low mobility and with a characteristic length scale. These regions of different mobility evolve in space and time. Importantly, the regions with high mobility can be identified from the dynamic susceptibility and are believed to facilitate structural relaxation in supercooled liquids and glasses. Quantification of dynamic heterogeneities can be carried out in more than one way, but it cannot be derived from $F_s(q,t)$.

Inhomogeneous MCT (IMCT) was developed (in part) to provide insight about the microscopic character of dynamic heterogeneities. Here we test, for the first time experimentally, IMCT predictions about dynamic heterogeneities. Specifically, we focus on the four-point susceptibility, $\chi_4(t)$, and the mean cluster-size of the most-mobile particles, $\langle N_c(t)\rangle$. In this subsection, we obtain these parameters from experiments and describe important trends; in the next subsection we will study their scaling properties to test predictions of IMCT.

The four-point susceptibility, $\chi_4(t)$, measures the temporal fluctuations of the two-point self-correlation function $Q_2(l, t)$; $\chi_4(l, t) = N(\langle Q_2(l, t)^2\rangle - \langle Q_2(l, t)\rangle^2)$.[1,50−55] Here, $Q_2(l, t) = \frac{1}{N}\sum_k^N \exp\frac{-\Delta\vec{r}_k(t)^2}{2l^2}$, where l is a preselected probing length scale, and the other symbols have their usual meanings. Thus, $\chi_4(t)$ quantifies the variance, or heterogeneity, in the displacements of particles for a given length scale l.[50,53−55,61] $\chi_4 \sim 0$ for simple liquid dynamics at high temperature. For supercooled liquids and glasses, however, $\chi_4(t)$ is strongly dependent on l, and it exhibits a maximum in the vicinity of the time scale, τ_4, when the dynamics are most heterogeneous. The peak amplitude of $\chi_4(t)$, i.e., $\chi_4(\tau_4)$, is proportional to number of particles participating in a typical particle cluster rearrangement. In Figure 4a, we show measured $\chi_4(t)$ versus lag time t as a function of ϕ; for each ϕ we use the value of l that maximizes $\chi_4(t)$. Notice that the sample dynamics become increasingly heterogeneous upon approaching the MCT crossover packing fraction, ϕ_c, i.e., as reflected in trend of $\chi_4(\tau_4)$ with ϕ. Note also, $\chi_4(t)$ at $\phi = 0.79$ exhibits two distinct peaks at two different times; based on IMCT predictions that we will discuss below, we believe that the second peak at the longer time scale signals when the dynamic heterogeneities are most prominent.

A second way of quantifying dynamic heterogeneity involves direct visualization of particle dynamics. First, the probability distribution of particle displacements $P(\Delta x\ (t))$ is measured for a given lag time t. The tails of this distribution are non-Gaussian.[37−39,58,62] This observation suggests that the particle dynamics are heterogeneous. Since fast particles are believed to be most involved in the pathways for structural relaxation in supercooled liquids and glasses, we identify the most-mobile particles associated with a given lag time t in the ensemble. To do this, we define a cutoff displacement, Δr_c, such that 10% of the particles have displacements (over lag time t), $|\Delta\vec{r}| \geq \Delta r_c$, see the Supporting Information for a representative probability distribution of displacements, $P(\Delta r(t))$. These most-mobile particles arise in the non-Gaussian tails of $P(\Delta x(t))$. After identification of these most-mobile particles, particle clusters are identified using standard nearest-neighbor algorithms.[37−39,58,62] (With this approach, we note that, for a given lag time t, the percentage of fast-moving particles in any given video frame (at any given time) may not be exactly 10%.[58])

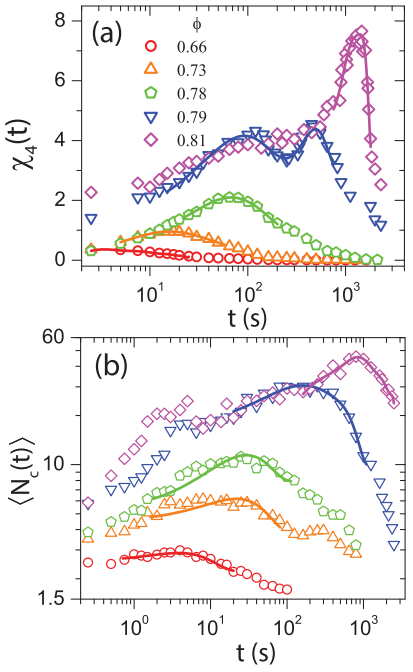

Figure 4. (a) Four-point susceptibility $\chi_4(t)$ versus lag time t at different packing area-fractions, ϕ. Note, the probing length scale l for each ϕ is chosen such that it maximizes $\chi_4(\tau_4)$ at that packing. (b) Mean cluster size, $\langle N_c(t)\rangle$, of the top 10% most-mobile particles for lag time t at different ϕ. The color codes in part b are the same as in part a. The solid lines in parts a and b are polynomial fits to the data around the peak.

After the most-mobile particle clusters are determined, we measure the temporal evolution of the mean-cluster size of most-mobile particles $\langle N_c(t)\rangle$; $\langle N_c(t)\rangle = \frac{\sum_{N_c} N_c^2 P(N_c)}{\sum_{N_c} N_c P(N_c)}$, where $P(N_c)$ is the probability of finding a cluster of size N_c. Figure 4b shows the plots of $\langle N_c(t)\rangle$ versus t as a function of ϕ. $\langle N_c(t)\rangle$ peaks in the vicinity of the time scale τ_c; at this time the dynamics are expected to be most-heterogeneous. The peak amplitude $\langle N_c(\tau_c)\rangle$ is explicitly associated with the number of particles participating in typical cooperative relaxation events. Figure 4b is thus analogous to Figure 4a, in the sense that similar trends with ϕ are observed for $\langle N_c(\tau_c)\rangle$, τ_c, and $\chi_4(\tau_4)$, τ_4, respectively.

Time-Dependent Growth of $\chi_4(t)$ and $\langle N_c(t)\rangle$: Explicit Tests of IMCT. Inhomogeneous MCT (IMCT) not only predicts growth of $\chi_4(\tau_4)$ and τ_4 upon approaching ϕ_c, but it also predicts the functional form of $\chi_4(t)$ in both the β-

DOI: 10.1021/acs.jpcb.9b03419
J. Phys. Chem. B 2019, 123, 5181−5188

relaxation and the early α-relaxation regimes.[57] The functional form of the growth of $\chi_4(t)$ in the early α-regime, in particular, has been used to discern the relative merits of competing glass transition formalisms.[57] IMCT predicts that $\chi_4(t)$ grows as a power law, $\chi_4(t) \sim t^{\mu}$, during both β- and early α-relaxation regimes; here the exponent $\mu = a$ for the β-relaxation regime, and $\mu = b$ for the early α-relaxation regime. Importantly, a and b are predicted to be the same as the MCT exponents we obtained from the decay profile of the dynamic self-intermediate scattering function, $F_s(q,t)$. These connections between model parameters have never been explored experimentally.

To test IMCT predictions in the early α-relaxation regime, we fit power laws to $\chi_4(t)$ in time intervals close to, but slightly earlier than, τ_4 (Figure 5(a)); we extract the power law exponent (μ) from these fits. Figure 5c shows the values of the exponent μ in the early α-relaxation regime as a function of ϕ (solid black squares in Figure 5c). Within experimental uncertainty, the extracted μ at different packing fractions (ϕ) are close to the von Schweidler exponent $b = 0.61 \pm 0.02$ (solid black line in Figure 5c). Unfortunately, poor temporal resolution in the β-relaxation regime prevented precision determination of μ for the short-time regime.

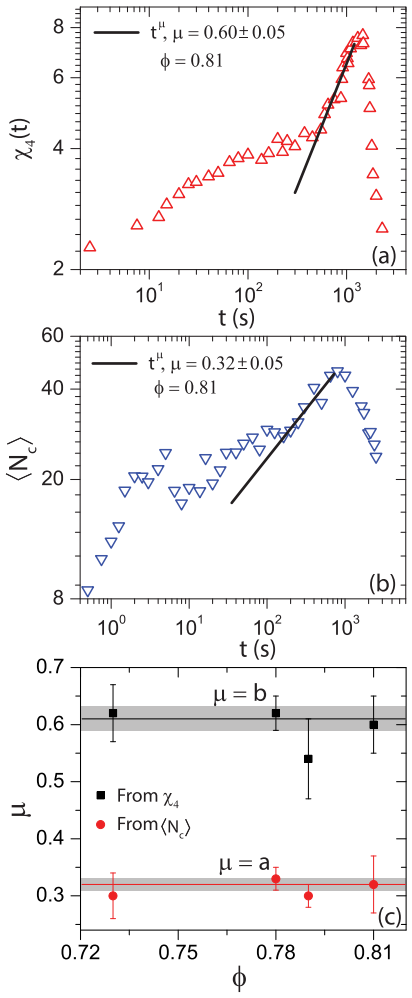

Figure 5. Log–log plot of (a) $\chi_4(t)$ and (b) $\langle N_c(t)\rangle$ versus lag time t for $\phi = 0.81$. From these curves, it is possible to extract the power law exponent μ in the early α-relaxation regime i.e. for the time intervals close to but less than τ_4 and τ_c. The black lines in parts a and b show $t^{0.62}$ and $t^{0.32}$ dependency, respectively. (c) Power law exponents, μ, extracted from $\chi_4(t)$ (solid black squares) and $\langle N_c(t)\rangle$ (solid red circles) plotted as a function of packing fraction, ϕ. The black and red lines correspond to $\mu = b$ and $\mu = a$, respectively. Recall, the mode coupling exponents, a and b, were extracted earlier from the self-intermediate scattering function $F_s(q,t)$. The gray shaded region around $\mu = b$ and $\mu = a$ corresponds to these MCT measurements including error bars.

Interestingly, as a brief aside, the consistency of μ in the early α-relaxation regime with the predictions of IMCT enabled us to ascertain which time scale among the two maxima in $\chi_4(t)$ (at $\phi = 0.79$) corresponds to the time at which the dynamic heterogeneities are most-prominent (Figure 4a). We determine μ by fitting to data obtained just before the first peak and just before the second peak; the fittings gave $\mu = 0.31 \pm 0.01$ and $\mu = 0.54 \pm 0.07$ for data near the first and second maxima, respectively. Within experimental uncertainty, only $\mu = 0.54 \pm 0.07$ is consistent with the predictions of IMCT. Therefore, at $\phi = 0.79$, the second peak ($\tau_4 = 440$ s) should be associated with the time at which the dynamic heterogeneities are most-prominent. Thus, for $\phi = 0.79$, $\tau_4 = 440$ s will be used in all further scaling analyses. Note also, at low ϕ ($\phi \leq 0.78$), we could fit a single power law to almost all the data for $t < \tau_4$ (except data at very small lag times); however, at higher ϕ ($\phi \geq 0.79$), the temporal range for power law fitting is small (Figure 4a and Figure 5a). The exponent μ, measured using data before the first peak at $\phi = 0.79$ ($\mu = 0.31 \pm 0.01$, $t = 110$ s), has a value close to the MCT critical exponent a; a is typically associated with β-relaxation. This observation could be a coincidence, or it could suggest a connection to processes at the short β-relaxation time scale; further investigation is needed.

Our findings about the functional form of $\chi_4(t)$ growth in the early α-relaxation regime corroborates predictions of IMCT. However, $\chi_4(t)$ is not the only way to characterize dynamic heterogeneity. As a check on the robustness of this finding, we investigate the functional form of another quantifier of dynamic heterogeneities in the early α-relaxation regime: the fast-particle mean cluster size $\langle N_c(t)\rangle$. The experiments and analyses reveal that $\langle N_c(t)\rangle$ grows as a power law in the early α-relaxation regime (Figure 5b), i.e., in the time intervals close to but just before τ_c (Figure 5b). The exponent μ is extracted from the fits. Figure 5c shows the values of μ as a function of packing fraction. Interestingly, while no predictions exist for μ in the early α-relaxation regime based on $\langle N_c(t)\rangle$, we find that the values of μ at different ϕ are close to the critical MCT decay law exponent a. In IMCT, this exponent (a) is typically associated with β-relaxation. It is surprising to note that while exponent μ in early α-relaxation regime for $\langle N_c(t)\rangle$ is close to the critical exponent a of the MCT (Figure 5c), the time scales at which $\langle N_c(t)\rangle$ peaks, τ_c, are close to (but always less than) long relaxation time scales, τ_4, obtained using the other quantifier of dynamic heterogeneities *i.e.* $\chi_4(t)$ (Figure 4). This suggests possible contributions of β-relaxation to $\langle N_c(t)\rangle$ processes. Unfortunately, the lack of a standard definition for estimating $\langle N_c(t)\rangle$ and the fact that the exponents μ in the early α-relaxation regime are sensitive to the definition of $\langle N_c(t)\rangle$ further precludes clear understanding of this unusual observation.[63] In the future, it is desirable to reconcile these observations within the purview of IMCT. (Note that at low ϕ ($\phi \leq 0.79$), we could fit a single power law to almost all the data for $t < \tau_4$, but at higher ϕ ($\phi = 0.81$), the temporal range for power law fitting is small (Figure 4b and Figure 5b).

DOI: 10.1021/acs.jpcb.9b03419
J. Phys. Chem. B 2019, 123, 5181−5188

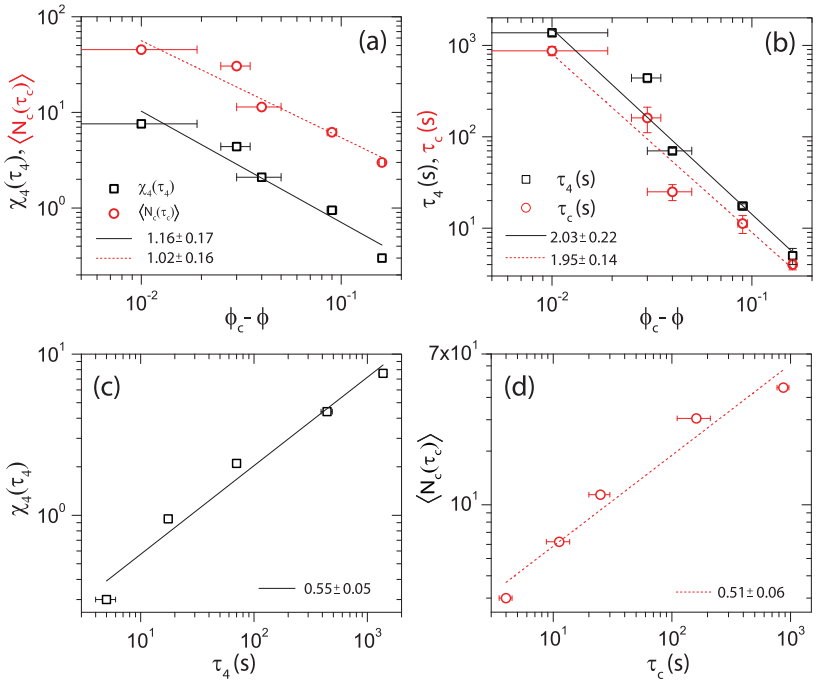

Figure 6. Log–log plot of the peak amplitude of the four-point susceptibility, $\chi_4(\tau_4)$ (open black squares), and the peak amplitude of mean cluster size of fast particles, $\langle N_c(\tau_c)\rangle$ (open red circles), versus $(\phi_c - \phi)$. (b) Log–log plot of τ_4 (open black squares) and τ_c (open red circles) versus $(\phi_c - \phi)$. In both (a) and (b), the mode coupling dynamic crossover packing fraction is set (from MCT measurements) to be $\phi_c = 0.82$. (c) $\chi_4(\tau_4)$ versus τ_4, and (d) $\langle N_c(\tau_c)\rangle$ versus τ_c. The error bars for estimation of $\chi_4(\tau_4)$ and $\langle N_c(\tau_c)\rangle$ are smaller than the symbol size. The black solid and red dashed lines in parts a–d are linear fits to the data.

Scaling of $\chi_4(\tau_4)$, τ_4, $\langle N_c(\tau_c)\rangle$, and τ_c in the Vicinity of ϕ_c. Lastly, we explore how $\chi_4(\tau_4)$, τ_4, $\langle N_c(\tau_c)\rangle$, and τ_c vary upon approaching the mode coupling crossover packing area-fraction, ϕ_c. Again, IMCT makes quantitative predictions about the scaling behavior of $\chi_4(\tau_4)$ and τ_4 with ϕ_c, but scientists involved with IMCT have not made predictions about $\langle N_c(\tau_c)\rangle$ and τ_c scaling with ϕ_c.

Figure 6a shows the plot of $\chi_4(\tau_4)$ (black squares) and $\langle N_c(\tau_c)\rangle$ (red circles) versus $(\phi_c - \phi)$. Both $\chi_4(\tau_4)$ and $\langle N_c(\tau_c)\rangle$ grow as a power law upon approaching ϕ_c. Specifically, $\chi_4(\tau_4) \propto (\phi_c - \phi)^{-\gamma_1^{DS}}$ and $\langle N_c(\tau_c)\rangle \propto (\phi_c - \phi)^{-\gamma_1^{MC}}$. Data fitting gives $\gamma_1^{DS} = 1.16 \pm 0.17$ and $\gamma_1^{MC} = 1.02 \pm 0.16$, where DS and MC represent dynamic susceptibility and mobile cluster, respectively. Within experimental error, the values of these exponents, γ_1^{DS} and γ_1^{MC}, agree with the theoretical prediction of IMCT, $\gamma_1 = 1$.

In Figure 6b, we plot the time scales τ_4 (black squares) and τ_c (red circles) versus $(\phi_c - \phi)$, respectively. Once again, we observe that both τ_4 and τ_c grow as a power law upon approaching ϕ_c. Specifically, $\tau_4 \propto (\phi_c - \phi)^{\gamma^{DS}}$ and $\tau_c \propto (\phi_c - \phi)^{\gamma^{MC}}$ with scaling exponents $\gamma^{DS} = 2.03 \pm 0.22$ and $\gamma^{MC} = 1.95 \pm 0.14$. Recall that the other long-time structural relaxation time scale (per MCT), τ_α, diverges as power law upon approaching ϕ_c with scaling exponent γ that we determined to be $\gamma = 2.43 \pm 0.02$. The measured γ^{DS} and γ^{MC} are thus less than γ, an observation consistent with Brownian dynamics simulations of Kob-Andersen Lennard-Jones mixtures.[46]

Finally, in parts c and d of Figure 6, we examine the variation of $\chi_4(\tau_4)$ with τ_4 and $\langle N_c(\tau_c)\rangle$ with τ_c, respectively. We find, albeit over limited dynamic range, that both $\chi_4(\tau_4)$ and $\langle N_c(\tau_c)\rangle$ exhibit power law behavior with increasing τ_4 and τ_c, respectively. Specifically, $\chi_4(\tau_4) \propto \tau_4^{\gamma_2^{DS}}$ and $\langle N_c(\tau_c)\rangle \propto \tau_c^{\gamma_2^{MC}}$. The scaling exponents are obtained from best fits and are $\gamma_2^{DS} = 0.55 \pm 0.05$ and $\gamma_2^{MC} = 0.51 \pm 0.06$. IMCT predicts $\gamma_2 = \frac{1}{\gamma} = 0.41 \pm 0.01$. Thus, the values of the measured exponents γ_2^{DS} and γ_2^{MC} are fairly close to the value predicted theoretically by IMCT.[64]

CONCLUSIONS

We have measured the spatiotemporal dynamics of quasi-two-dimensional colloidal supercooled liquids. We determined the MCT exponents (a, b, γ) and the structural relaxation time scale (τ_α) for these systems, and the scaling of $\tau_\alpha^{-1/\gamma}$ with ϕ gave the mode coupling dynamic crossover packing area-fraction, ϕ_c. Next, we quantified dynamic heterogeneities in these samples using the four-point dynamic susceptibility, $\chi_4(t)$, and the mean cluster size of the top 10% most mobile particles ($\langle N_c(t)\rangle$). Both $\chi_4(t)$ and $\langle N_c(t)\rangle$ grow as power laws in the early α-relaxation regime. Consistent with the predictions of inhomogeneous MCT (IMCT), the power law exponent, μ, extracted from $\chi_4(t)$ is observed to be close to the MCT exponent b and is clearly different from the predictions of diffusing defect models in three dimensions, which give $\mu = 2$.[57] The exponents μ extracted from $\langle N_c(t)\rangle$ in the early α-relaxation regime at different packing fractions are close to the MCT exponent a; these new experimental observations should stimulate development/extension of theoretical formalisms that predict the functional form of growth of other quantifiers of dynamic heterogeneities such as $\langle N_c(t)\rangle$. In addition, we measured time scales associated with these dynamic heterogeneities, i.e., τ_4 and τ_c, and we found that they grow as power laws upon approaching ϕ_c with power law exponents smaller than the MCT exponent γ. Furthermore, and again consistent with IMCT predictions, $\chi_4(\tau_4)$ and $\langle N_c(\tau_c)\rangle$ are observed to

DOI: 10.1021/acs.jpcb.9b03419
J. Phys. Chem. B 2019, 123, 5181–5188

diverge as power law with $(\phi_c - \phi)$, with exponent $\gamma_1 \sim 1$. Finally, $\chi_4(\tau_4)$ and $\langle N_c(\tau_c)\rangle$ grow as power laws with increasing τ_4 and τ_c, respectively, with exponents close to $\gamma_2 \sim \frac{1}{\gamma}$. Taken together, our experimental observations suggest that the dynamics in the supercooled colloidal suspensions are well captured by the *inhomogeneous* mode coupling theory (IMCT); they are not consistent with other models such as the diffusive defect model or the kinetic constrained models with noncooperative defects (i.e., based on the values of μ in the early α-relaxation regime).[57]

■ ASSOCIATED CONTENT

Supporting Information

The Supporting Information is available free of charge on the ACS Publications website at DOI: 10.1021/acs.jpcb.9b03419.

Representative probability distribution of displacements (PDF)

■ AUTHOR INFORMATION

Corresponding Author

*(A.G.Y.) E-mail: yodh@physics.upenn.edu.

ORCID

A. G. Yodh: 0000-0003-4744-2706

Notes

The authors declare no competing financial interest.

■ ACKNOWLEDGMENTS

We are delighted to contribute this paper to the Hai-Lung Dai Festschrift. Hai-Lung is a truly first-rank scientist who has been a wonderful colleague to one of us (A.G.Y.) for more than 30 years. For those of us lucky enough to know him, Hai-Lung's enthusiasm, wisdom, and steady hand have been an inspiration. We also thank Kevin Aptowicz, Remi Dreyfus, Peter Collings, and Xiaoguang Ma for helpful discussions. C.K.M and A.G.Y. gratefully acknowledge financial support from the National Science Foundation through DMR16-07378, the MRSEC DMR-1720530 including its Optical Microscopy Shared Experimental Facility, and NASA through NNX13AL27G.

■ REFERENCES

(1) Berthier, L.; Biroli, G.; Bouchaud, J.-P.; Cipelletti, L.; van Saarloos, W. *Dynamical heterogeneities in glasses, colloids, and granular media* **2011**, *150*, 1 DOI: 10.1093/acprof:oso/9780199691470.001.0001.

(2) Götze, W.; Sjögren, L. Relaxation processes in supercooled liquids. *Rep. Prog. Phys.* **1992**, *55*, 241.

(3) Angell, C. A. Formation of glasses from liquids and biopolymers. *Science* **1995**, *267*, 1924−1935.

(4) Angell, C. A. Perspective on the glass transition. *J. Phys. Chem. Solids* **1988**, *49*, 863−871.

(5) Dyre, J. C. Colloquium: The glass transition and elastic models of glass-forming liquids. *Rev. Mod. Phys.* **2006**, *78*, 953.

(6) Kauzmann, W. The nature of the glassy state and the behavior of liquids at low temperatures. *Chem. Rev.* **1948**, *43*, 219−256.

(7) Berthier, L.; Biroli, G. Theoretical perspective on the glass transition and amorphous materials. *Rev. Mod. Phys.* **2011**, *83*, 587.

(8) Gokhale, S.; Sood, A.; Ganapathy, R. Deconstructing the glass transition through critical experiments on colloids. *Adv. Phys.* **2016**, *65*, 363−452.

(9) Stillinger, F. H. A topographic view of supercooled liquids and glass formation. *Science* **1995**, *267*, 1935−1939.

(10) Debenedetti, P. G.; Stillinger, F. H. Supercooled liquids and the glass transition. *Nature* **2001**, *410*, 259.

(11) Zhang, Z.; Xu, N.; Chen, D. T.; Yunker, P.; Alsayed, A. M.; Aptowicz, K. B.; Habdas, P.; Liu, A. J.; Nagel, S. R.; Yodh, A. G. Thermal vestige of the zero-temperature jamming transition. *Nature* **2009**, *459*, 230.

(12) Leheny, R. L.; Menon, N.; Nagel, S. R.; Long Price, D.; Suzuya, K.; Thiyagarajan, P. Structural studies of an organic liquid through the glass transition. *J. Chem. Phys.* **1996**, *105*, 7783−7794.

(13) Cohen, M. H.; Turnbull, D. Molecular transport in liquids and glasses. *J. Chem. Phys.* **1959**, *31*, 1164.

(14) Turnbull, D.; Cohen, M. H. Free-volume model of the amorphous phase: glass transition. *J. Chem. Phys.* **1961**, *34*, 120.

(15) Stillinger, F. H.; Weber, T. A. Hidden structure in liquids. *Phys. Rev. A: At., Mol., Opt. Phys.* **1982**, *25*, 978.

(16) Stillinger, F. H.; Weber, T. A. Dynamics of structural transitions in liquids. *Phys. Rev. A: At., Mol., Opt. Phys.* **1983**, *28*, 2408.

(17) Gibbs, J. H.; DiMarzio, E. A. Nature of the glass transition and the glassy state. *J. Chem. Phys.* **1958**, *28*, 373.

(18) Adam, G.; Gibbs, J. H. On the temperature dependence of cooperative relaxation properties in glass-forming liquids. *J. Chem. Phys.* **1965**, *43*, 139.

(19) Bengtzelius, U.; Götze, W.; Sjölander, A. Dynamics of supercooled liquids and the glass transition. *J. Phys. C: Solid State Phys.* **1984**, *17*, 5915.

(20) Bosse, J.; Götze, W.; Lücke, M. Mode-coupling theory of simple classical liquids. *Phys. Rev. A: At., Mol., Opt. Phys.* **1978**, *17*, 434.

(21) Ritort, F.; Sollich, P. Glassy dynamics of kinetically constrained models. *Adv. Phys.* **2003**, *52*, 219−342.

(22) Kirkpatrick, T.; Thirumalai, D. Dynamics of the structural glass transition and the p-spin-interaction spin-glass model. *Phys. Rev. Lett.* **1987**, *58*, 2091.

(23) Kirkpatrick, T.; Thirumalai, D. p-spin-interaction spin-glass models: Connections with the structural glass problem. *Phys. Rev. B: Condens. Matter Mater. Phys.* **1987**, *36*, 5388.

(24) Kirkpatrick, T.; Thirumalai, D.; Wolynes, P. G. Scaling concepts for the dynamics of viscous liquids near an ideal glassy state. *Phys. Rev. A: At., Mol., Opt. Phys.* **1989**, *40*, 1045.

(25) Garrahan, J. P.; Chandler, D. Geometrical explanation and scaling of dynamical heterogeneities in glass forming systems. *Phys. Rev. Lett.* **2002**, *89*, 035704.

(26) Garrahan, J. P.; Chandler, D. Coarse-grained microscopic model of glass formers. *Proc. Natl. Acad. Sci. U. S. A.* **2003**, *100*, 9710.

(27) Szamel, G. Mode-coupling theory and beyond: A diagrammatic approach. *Prog. Theor. Exp. Phys.* **2013**, *2013*, 012J01.

(28) Kob, W. The mode-coupling theory of the glass transition. *arXiv preprint cond-mat/9702073*, 1997.

(29) Das, S. P. Mode-coupling theory and the glass transition in supercooled liquids. *Rev. Mod. Phys.* **2004**, *76*, 785.

(30) Gleim, T.; Kob, W. The β-relaxation dynamics of a simple liquid. *Eur. Phys. J. B* **2000**, *13*, 83−86.

(31) Gotze, W. The scaling functions for the β-relaxation process of supercooled liquids and glasses. *J. Phys.: Condens. Matter* **1990**, *2*, 8485.

(32) Brumer, Y.; Reichman, D. R. Mean-field theory, mode-coupling theory, and the onset temperature in supercooled liquids. *Phys. Rev. E* **2004**, *69*, 041202.

(33) Stevenson, J. D.; Schmalian, J.; Wolynes, P. G. The shapes of cooperatively rearranging regions in glass-forming liquids. *Nat. Phys.* **2006**, *2*, 268.

(34) Hall, R. W.; Wolynes, P. G. Intermolecular forces and the glass transition. *J. Phys. Chem. B* **2008**, *112*, 301−312.

(35) Bhattacharyya, S. M.; Bagchi, B.; Wolynes, P. G. Facilitation, complexity growth, mode coupling, and activated dynamics in supercooled liquids. *Proc. Natl. Acad. Sci. U. S. A.* **2008**, *105*, 16077.

(36) Lubchenko, V.; Wolynes, P. G. Aging, jamming, and the limits of stability of amorphous solids. *J. Phys. Chem. B* **2018**, *122*, 3280−3295.

(37) Mishra, C. K.; Rangarajan, A.; Ganapathy, R. Two-step glass transition induced by attractive interactions in quasi-two-dimensional suspensions of ellipsoidal particles. *Phys. Rev. Lett.* **2013**, *110*, 188301.

(38) Hima Nagamanasa, K.; Gokhale, S.; Sood, A.; Ganapathy, R. Direct measurements of growing amorphous order and non-monotonic dynamic correlations in a colloidal glass-former. *Nat. Phys.* **2015**, *11*, 403.
(39) Zheng, Z.; Ni, R.; Wang, F.; Dijkstra, M.; Wang, Y.; Han, Y. Structural signatures of dynamic heterogeneities in monolayers of colloidal ellipsoids. *Nat. Commun.* **2014**, *5*, 3829.
(40) Li, G.; Du, W. M.; Chen, X. K.; Cummins, H. Z.; Tao, N. J. Testing mode-coupling predictions for α and β relaxation in $Ca_{0.4}K_{0.6}(NO_3)_{1.4}$ near the liquid-glass transition by light scattering. *Phys. Rev. A: At., Mol., Opt. Phys.* **1992**, *45*, 3867.
(41) Hinze, G.; Brace, D. D.; Gottke, S.; Fayer, M. A detailed test of mode-coupling theory on all time scales: Time domain studies of structural relaxation in a supercooled liquid. *J. Chem. Phys.* **2000**, *113*, 3723−3733.
(42) Pham, K. N.; Puertas, A. M.; Bergenholtz, J.; Egelhaaf, S. U.; Moussaıd, A.; Pusey, P. N.; Schofield, A. B.; Cates, M. E.; Fuchs, M.; Poon, W. C. Multiple glassy states in a simple model system. *Science* **2002**, *296*, 104−106.
(43) Pham, K.; Egelhaaf, S.; Pusey, P.; Poon, W. C. Glasses in hard spheres with short-range attraction. *Phys. Rev. E* **2004**, *69*, 011503.
(44) Van Megen, W.; Underwood, S.; Pusey, P. Nonergodicity parameters of colloidal glasses. *Phys. Rev. Lett.* **1991**, *67*, 1586.
(45) Brambilla, G.; El Masri, D.; Pierno, M.; Berthier, L.; Cipelletti, L.; Petekidis, G.; Schofield, A. B. Probing the equilibrium dynamics of colloidal hard spheres above the mode-coupling glass transition. *Phys. Rev. Lett.* **2009**, *102*, 085703.
(46) Szamel, G.; Flenner, E. Four-point susceptibility of a glass-forming binary mixture: Brownian dynamics. *Phys. Rev. E* **2006**, *74*, 021507.
(47) Kob, W.; Andersen, H. C. Testing mode-coupling theory for a supercooled binary Lennard-Jones mixture I: The van Hove correlation function. *Phys. Rev. E: Stat. Phys., Plasmas, Fluids, Relat. Interdiscip. Top.* **1995**, *51*, 4626.
(48) Frenkel, D.; Ernst, M. Simulation of diffusion in a two-dimensional lattice-gas cellular automaton: A test of mode-coupling theory. *Phys. Rev. Lett.* **1989**, *63*, 2165.
(49) Berthier, L.; Tarjus, G. Critical test of the mode-coupling theory of the glass transition. *Phys. Rev. E* **2010**, *82*, 031502.
(50) Zhang, Z.; Yunker, P. J.; Habdas, P.; Yodh, A. Cooperative rearrangement regions and dynamical heterogeneities in colloidal glasses with attractive versus repulsive interactions. *Phys. Rev. Lett.* **2011**, *107*, 208303.
(51) Dasgupta, C.; Indrani, A.; Ramaswamy, S.; Phani, M. Is there a growing correlation length near the glass transition? *Europhys. Lett.* **1991**, *15*, 307.
(52) Donati, C.; Glotzer, S. C.; Poole, P. H. Growing spatial correlations of particle displacements in a simulated liquid on cooling toward the glass transition. *Phys. Rev. Lett.* **1999**, *82*, 5064.
(53) Keys, A. S.; Abate, A. R.; Glotzer, S. C.; Durian, D. J. Measurement of growing dynamical length scales and prediction of the jamming transition in a granular material. *Nat. Phys.* **2007**, *3*, 260.
(54) Abate, A. R.; Durian, D. Topological persistence and dynamical heterogeneities near jamming. *Phys. Rev. E* **2007**, *76*, 021306.
(55) Dauchot, O.; Marty, G.; Biroli, G. Dynamical heterogeneity close to the jamming transition in a sheared granular material. *Phys. Rev. Lett.* **2005**, *95*, 265701.
(56) Biroli, G.; Bouchaud, J.-P.; Miyazaki, K.; Reichman, D. R. Inhomogeneous mode-coupling theory and growing dynamic length in supercooled liquids. *Phys. Rev. Lett.* **2006**, *97*, 195701.
(57) Toninelli, C.; Wyart, M.; Berthier, L.; Biroli, G.; Bouchaud, J.-P. Dynamical susceptibility of glass formers: Contrasting the predictions of theoretical scenarios. *Phys. Rev. E* **2005**, *71*, 041505.
(58) Weeks, E. R.; Crocker, J. C.; Levitt, A. C.; Schofield, A.; Weitz, D. A. Three-dimensional direct imaging of structural relaxation near the colloidal glass transition. *Science* **2000**, *287*, 627−631.
(59) Crocker, J. C.; Grier, D. G. Methods of digital video microscopy for colloidal studies. *J. Colloid Interface Sci.* **1996**, *179*, 298−310.
(60) Flenner, E.; Szamel, G. Dynamic heterogeneity in a glass forming fluid: Susceptibility, structure factor, and correlation length. *Phys. Rev. Lett.* **2010**, *105*, 217801.
(61) Yunker, P.; Zhang, Z.; Yodh, A. G. Observation of the disorder-induced crystal-to-glass transition. *Phys. Rev. Lett.* **2010**, *104*, 015701.
(62) Mishra, C. K.; Ganapathy, R. Shape of dynamical heterogeneities and fractional Stokes-Einstein and Stokes-Einstein-Debye relations in quasi-two-dimensional suspensions of colloidal ellipsoids. *Phys. Rev. Lett.* **2015**, *114*, 198302.
(63) Instead of particle average mean cluster size, $\langle N_c(t)\rangle = \frac{\sum_{N_c} N_c^2 P(N_c)}{\sum_{N_c} N_c P(N_c)}$, we have also computed clustered average mean size, $\langle N_c(t)\rangle = \sum_{N_c} N_c P(N_c)$. Irrespective of the definition used, the time at which $\langle N_c(t)\rangle$ peaks remains the same. However, the values of exponent μ in early α-relaxation regime at different packing fraction are observed to be larger when the former definition is used.
(64) At times, $Q_2(\tau_4)$ is used to normalize $\chi_4(\tau_4)$, $\frac{\chi_4(\tau_4)}{Q_2(\tau_4)}$, that converts $\chi_4(\tau_4)$ to the number of particles participating in the cage rearrangement events. However, $Q_2(\tau_4)$ was found to be constant for all packing area fractions ($Q_2(\tau_4) = 0.23 \pm 0.03$), and thus the scaling of $\chi_4(\tau_4)$ with $(\phi_c - \phi)$ or with τ_4 remained invariant even after normalization.

DOI: 10.1021/acs.jpcb.9b03419
J. Phys. Chem. B 2019, 123, 5181−5188